ELSEVIER

Measurement of trilinear gauge boson couplings WWV, ($V \equiv Z, \gamma$) in e^+e^- collisions at 189 GeV

DELPHI Collaboration

P. Abreu [u], W. Adam [ax], T. Adye [aj], P. Adzic [k], Z. Albrecht [q], T. Alderweireld [b],
G.D. Alekseev [p], R. Alemany [i], T. Allmendinger [q], P.P. Allport [v], S. Almehed [x],
U. Amaldi [ab], N. Amapane [as], S. Amato [au], E. Anashkin [ai], E.G. Anassontzis [c],
P. Andersson [ar], A. Andreazza [aa], S. Andringa [u], N. Anjos [u], P. Antilogus [y], W.-D. Apel [q],
Y. Arnoud [n], B. Åsman [ar], J.-E. Augustin [w], A. Augustinus [i], P. Baillon [i],
A. Ballestrero [as], P. Bambade [i,s], F. Barao [u], G. Barbiellini [at], R. Barbier [y], D.Y. Bardin [p],
G. Barker [q], A. Baroncelli [al], M. Battaglia [o], M. Baubillier [w], K.-H. Becks [az], M. Begalli [f],
A. Behrmann [az], Yu. Belokopytov [i], K. Belous [ap], N.C. Benekos [ae], A.C. Benvenuti [e],
C. Berat [n], M. Berggren [w], L. Berntzon [ar], D. Bertrand [b], M. Besancon [am], N. Besson [am],
M.S. Bilenky [p], D. Bloch [j], H.M. Blom [ad], L. Bol [q], M. Bonesini [ab], M. Boonekamp [am],
P.S.L. Booth [v], G. Borisov [s], C. Bosio [ao], O. Botner [av], E. Boudinov [ad], B. Bouquet [s],
T.J.V. Bowcock [v], I. Boyko [p], I. Bozovic [k], M. Bozzo [m], M. Bracko [aq], P. Branchini [al],
R.A. Brenner [av], P. Bruckman [i], J.-M. Brunet [h], L. Bugge [af], P. Buschmann [az],
M. Caccia [aa], M. Calvi [ab], T. Camporesi [i], V. Canale [ak], F. Carena [i], L. Carroll [v],
C. Caso [m], M.V. Castillo Gimenez [aw], A. Cattai [i], F.R. Cavallo [e], M. Chapkin [ap],
Ph. Charpentier [i], P. Checchia [ai], G.A. Chelkov [p], R. Chierici [as], P. Chliapnikov [i,ap],
P. Chochula [g], V. Chorowicz [y], J. Chudoba [ac], K. Cieslik [r], P. Collins [i], R. Contri [m],
E. Cortina [aw], G. Cosme [s], F. Cossutti [i], M. Costa [aw], H.B. Crawley [a], D. Crennell [aj],
J. Croix [j], G. Crosetti [m], J. Cuevas Maestro [ag], S. Czellar [o], J. D'Hondt [b], J. Dalmau [ar],
M. Davenport [i], W. Da Silva [w], G. Della Ricca [at], P. Delpierre [z], N. Demaria [as],
A. De Angelis [at], W. De Boer [q], C. De Clercq [b], B. De Lotto [at], A. De Min [i],
L. De Paula [au], H. Dijkstra [i], L. Di Ciaccio [ak], K. Doroba [ay], M. Dracos [j], J. Drees [az],
M. Dris [ae], G. Eigen [d], T. Ekelof [av], M. Ellert [av], M. Elsing [i], J.-P. Engel [j],
M. Espirito Santo [i], G. Fanourakis [k], D. Fassouliotis [k], M. Feindt [q], J. Fernandez [an],
A. Ferrer [aw], E. Ferrer-Ribas [s], F. Ferro [m], A. Firestone [a], U. Flagmeyer [az], H. Foeth [i],
E. Fokitis [ae], F. Fontanelli [m], B. Franek [aj], A.G. Frodesen [d], R. Fruhwirth [ax],
F. Fulda-Quenzer [s], J. Fuster [aw], A. Galloni [v], D. Gamba [as], S. Gamblin [s],
M. Gandelman [au], C. Garcia [aw], C. Gaspar [i], M. Gaspar [au], U. Gasparini [ai], Ph. Gavillet [i],
E.N. Gazis [ae], D. Gele [j], T. Geralis [k], N. Ghodbane [y], I. Gil [aw], F. Glege [az], R. Gokieli [i,ay],

B. Golob [i,aq], G. Gomez-Ceballos [an], P. Goncalves [u], I. Gonzalez Caballero [an],
G. Gopal [aj], L. Gorn [a], Yu. Gouz [ap], V. Gracco [m], J. Grahl [a], E. Graziani [al],
G. Grosdidier [s], K. Grzelak [ay], J. Guy [aj], C. Haag [q], F. Hahn [i], S. Hahn [az], S. Haider [i],
A. Hallgren [av], K. Hamacher [az], J. Hansen [af], F.J. Harris [ah], S. Haug [af], F. Hauler [q],
V. Hedberg [i,x], S. Heising [q], J.J. Hernandez [aw], P. Herquet [b], H. Herr [i], O. Hertz [q],
E. Higon [aw], S.-O. Holmgren [ar], P.J. Holt [ah], S. Hoorelbeke [b], M. Houlden [v], J. Hrubec [ax],
G.J. Hughes [v], K. Hultqvist [i,ar], J.N. Jackson [v], R. Jacobsson [i], P. Jalocha [r], Ch. Jarlskog [x],
G. Jarlskog [x], P. Jarry [am], B. Jean-Marie [s], D. Jeans [ah], E.K. Johansson [ar], P. Jonsson [y],
C. Joram [i], P. Juillot [j], L. Jungermann [q], F. Kapusta [w], K. Karafasoulis [k], S. Katsanevas [y],
E.C. Katsoufis [ae], R. Keranen [q], G. Kernel [aq], B.P. Kersevan [aq], Yu. Khokhlov [ap],
B.A. Khomenko [p], N.N. Khovanski [p], A. Kiiskinen [o], B. King [v], A. Kinvig [v], N.J. Kjaer [i],
O. Klapp [az], P. Kluit [ad], P. Kokkinias [k], V. Kostioukhine [ap], C. Kourkoumelis [c],
O. Kouznetsov [p], M. Krammer [ax], E. Kriznic [aq], Z. Krumstein [p], P. Kubinec [g],
M. Kucharczyk [r], J. Kurowska [ay], J.W. Lamsa [a], J.-P. Laugier [am], G. Leder [ax], F. Ledroit [n],
L. Leinonen [ar], A. Leisos [k], R. Leitner [ac], G. Lenzen [az], V. Lepeltier [s], T. Lesiak [r],
M. Lethuillier [y], J. Libby [ah], W. Liebig [az], D. Liko [i], A. Lipniacka [ar], I. Lippi [ai],
J.G. Loken [ah], J.H. Lopes [au], J.M. Lopez [an], R. Lopez-Fernandez [n], D. Loukas [k],
P. Lutz [am], L. Lyons [ah], J. MacNaughton [ax], J.R. Mahon [f], A. Maio [u], A. Malek [az],
S. Maltezos [ae], V. Malychev [p], F. Mandl [ax], J. Marco [an], R. Marco [an], B. Marechal [au],
M. Margoni [ai], J.-C. Marin [i], C. Mariotti [i], A. Markou [k], C. Martinez-Rivero [i],
S. Marti i Garcia [i], J. Masik [l], N. Mastroyiannopoulos [k], F. Matorras [an], C. Matteuzzi [ab],
G. Matthiae [ak], F. Mazzucato [ai], M. Mazzucato [ai], M. Mc Cubbin [v], R. Mc Kay [a],
R. Mc Nulty [v], G. Mc Pherson [v], E. Merle [n], C. Meroni [aa], W.T. Meyer [a], E. Migliore [i],
L. Mirabito [y], W.A. Mitaroff [ax], U. Mjoernmark [x], T. Moa [ar], M. Moch [q], K. Moenig [i,1],
M.R. Monge [m], J. Montenegro [ad], D. Moraes [au], P. Morettini [m], G. Morton [ah],
U. Mueller [az], K. Muenich [az], M. Mulders [ad], L.M. Mundim [f], W.J. Murray [aj], B. Muryn [r],
G. Myatt [ah], T. Myklebust [af], M. Nassiakou [k], F.L. Navarria [e], K. Nawrocki [ay], P. Negri [ab],
S. Nemecek [l], N. Neufeld [ax], R. Nicolaidou [am], P. Niezurawski [ay], M. Nikolenko [j,p],
V. Nomokonov [o], A. Nygren [x], V. Obraztsov [ap], A.G. Olshevski [p], A. Onofre [u],
R. Orava [o], K. Osterberg [i], A. Ouraou [am], A. Oyanguren [aw], M. Paganoni [ab], S. Paiano [e],
R. Pain [w], R. Paiva [u], J. Palacios [ah], H. Palka [r], Th.D. Papadopoulou [ae], L. Pape [i],
C. Parkes [i], F. Parodi [m], U. Parzefall [v], A. Passeri [al], O. Passon [az], T. Pavel [x],
M. Pegoraro [ai], L. Peralta [u], V. Perepelitsa [aw], M. Pernicka [ax], A. Perrotta [e], C. Petridou [at],
A. Petrolini [m], H.T. Phillips [aj], F. Pierre [am], M. Pimenta [u], E. Piotto [aa], T. Podobnik [aq],
V. Poireau [am], M.E. Pol [f], G. Polok [r], P. Poropat [at], V. Pozdniakov [p], P. Privitera [ak],
N. Pukhaeva [p], A. Pullia [ab], D. Radojicic [ah], S. Ragazzi [ab], H. Rahmani [ae], P.N. Ratoff [t],
A.L. Read [af], P. Rebecchi [i], N.G. Redaelli [ab], M. Regler [ax], J. Rehn [q], D. Reid [ad],
R. Reinhardt [az], P.B. Renton [ah], L.K. Resvanis [c], F. Richard [s], J. Ridky [l], G. Rinaudo [as],

I. Ripp-Baudot [j], A. Romero [as], P. Ronchese [ai], E.I. Rosenberg [a], P. Rosinsky [g],
P. Roudeau [s], T. Rovelli [e], V. Ruhlmann-Kleider [am], A. Ruiz [an], H. Saarikko [o],
Y. Sacquin [am], A. Sadovsky [p], G. Sajot [n], L. Salmi [o], J. Salt [aw], D. Sampsonidis [k],
M. Sannino [m], A. Savoy-Navarro [w], C. Schwanda [ax], Ph. Schwemling [w], B. Schwering [az],
U. Schwickerath [q], F. Scuri [at], P. Seager [t], Y. Sedykh [p], A.M. Segar [ah], R. Sekulin [aj],
R.C. Shellard [f], M. Siebel [az], L. Simard [am], F. Simonetto [ai], A.N. Sisakian [p], G. Smadja [y],
N. Smirnov [ap], O. Smirnova [x], G.R. Smith [aj], O. Solovianov [ap], A. Sopczak [q],
R. Sosnowski [ay], T. Spassov [i], E. Spiriti [al], S. Squarcia [m], C. Stanescu [al], M. Stanitzki [q],
K. Stevenson [ah], A. Stocchi [s], J. Strauss [ax], R. Strub [j], B. Stugu [d], M. Szczekowski [ay],
M. Szeptycka [ay], T. Tabarelli [ab], A. Taffard [v], O. Tchikilev [ap], F. Tegenfeldt [av],
F. Terranova [ab], J. Timmermans [ad], N. Tinti [e], L.G. Tkatchev [p], M. Tobin [v], S. Todorova [i],
B. Tome [u], A. Tonazzo [i], L. Tortora [al], P. Tortosa [aw], D. Treille [i], G. Tristram [h],
M. Trochimczuk [ay], C. Troncon [aa], M.-L. Turluer [am], I.A. Tyapkin [p], P. Tyapkin [x],
S. Tzamarias [k], O. Ullaland [i], V. Uvarov [ap], G. Valenti [i,e], E. Vallazza [at], P. Van Dam [ad],
W. Van den Boeck [b], W.K. Van Doninck [b], J. Van Eldik [i,ad], A. Van Lysebetten [b],
N. van Remortel [b], I. Van Vulpen [ad], G. Vegni [aa], L. Ventura [ai], W. Venus [aj,i],
F. Verbeure [b], P. Verdier [y], M. Verlato [ai], L.S. Vertogradov [p], V. Verzi [aa], D. Vilanova [am],
L. Vitale [at], E. Vlasov [ap], A.S. Vodopyanov [p], G. Voulgaris [c], V. Vrba [l], H. Wahlen [az],
A.J. Washbrook [v], C. Weiser [i], D. Wicke [i], J.H. Wickens [b], G.R. Wilkinson [ah],
M. Winter [j], M. Witek [r], G. Wolf [i], J. Yi [a], O. Yushchenko [ap], A. Zalewska [r],
P. Zalewski [ay], D. Zavrtanik [aq], E. Zevgolatakos [k], N.I. Zimin [p,x], A. Zintchenko [p],
Ph. Zoller [j], G. Zumerle [ai], M. Zupan [k]

[a] *Department of Physics and Astronomy, Iowa State University, Ames, IA 50011-3160, USA*
[b] *Physics Department, Univ. Instelling Antwerpen, Universiteitsplein 1, B-2610 Antwerpen,*
and IIHE, ULB-VUB, Pleinlaan 2, B-1050 Brussels,
and Faculté des Sciences, Univ. de l'Etat Mons, Av. Maistriau 19, B-7000 Mons, Belgium
[c] *Physics Laboratory, University of Athens, Solonos Str. 104, GR-10680 Athens, Greece*
[d] *Department of Physics, University of Bergen, Allégaten 55, NO-5007 Bergen, Norway*
[e] *Dipartimento di Fisica, Università di Bologna and INFN, Via Irnerio 46, IT-40126 Bologna, Italy*
[f] *Centro Brasileiro de Pesquisas Físicas, rua Xavier Sigaud 150, BR-22290 Rio de Janeiro,*
and Depto. de Física, Pont. Univ. Católica, C.P. 38071 BR-22453 Rio de Janeiro,
and Inst. de Física, Univ. Estadual do Rio de Janeiro, rua São Francisco Xavier 524, Rio de Janeiro, Brazil
[g] *Comenius University, Faculty of Mathematics and Physics, Mlynska Dolina, SK-84215 Bratislava, Slovakia*
[h] *Collège de France, Lab. de Physique Corpusculaire, IN2P3-CNRS, FR-75231 Paris Cedex 05, France*
[i] *CERN, CH-1211 Geneva 23, Switzerland*
[j] *Institut de Recherches Subatomiques, IN2P3-CNRS/ULP-BP20, FR-67037 Strasbourg Cedex, France*
[k] *Institute of Nuclear Physics, N.C.S.R. Demokritos, P.O. Box 60228, GR-15310 Athens, Greece*
[l] *FZU, Inst. of Phys. of the C.A.S. High Energy Physics Division, Na Slovance 2, CZ-180 40, Praha 8, Czech Republic*
[m] *Dipartimento di Fisica, Università di Genova and INFN, Via Dodecaneso 33, IT-16146 Genova, Italy*
[n] *Institut des Sciences Nucléaires, IN2P3-CNRS, Université de Grenoble 1, FR-38026 Grenoble Cedex, France*
[o] *Helsinki Institute of Physics, HIP, P.O. Box 9, FI-00014 Helsinki, Finland*
[p] *Joint Institute for Nuclear Research, Dubna, Head Post Office, P.O. Box 79, RU-101 000 Moscow, Russian Federation*
[q] *Institut für Experimentelle Kernphysik, Universität Karlsruhe, Postfach 6980, DE-76128 Karlsruhe, Germany*
[r] *Institute of Nuclear Physics and University of Mining and Metalurgy, Ul. Kawiory 26a, PL-30055 Krakow, Poland*
[s] *Université de Paris-Sud, Lab. de l'Accélérateur Linéaire, IN2P3-CNRS, Bât. 200, FR-91405 Orsay Cedex, France*
[t] *School of Physics and Chemistry, University of Lancaster, Lancaster LA1 4YB, UK*

[u] *LIP, IST, FCUL - Av. Elias Garcia, 14-1º, PT-1000 Lisboa Codex, Portugal*
[v] *Department of Physics, University of Liverpool, P.O. Box 147, Liverpool L69 3BX, UK*
[w] *LPNHE, IN2P3-CNRS, Univ. Paris VI et VII, Tour 33 (RdC), 4 place Jussieu, FR-75252 Paris Cedex 05, France*
[x] *Department of Physics, University of Lund, Sölvegatan 14, SE-223 63 Lund, Sweden*
[y] *Université Claude Bernard de Lyon, IPNL, IN2P3-CNRS, FR-69622 Villeurbanne Cedex, France*
[z] *Univ. d'Aix-Marseille II-CPP, IN2P3-CNRS, FR-13288 Marseille Cedex 09, France*
[aa] *Dipartimento di Fisica, Università di Milano and INFN-MILANO, Via Celoria 16, IT-20133 Milan, Italy*
[ab] *Dipartimento di Fisica, Univ. di Milano-Bicocca and INFN-MILANO, Piazza delle Scienze 2, IT-20126 Milan, Italy*
[ac] *IPNP of MFF, Charles Univ., Areal MFF, V Holesovickach 2, CZ-180 00, Praha 8, Czech Republic*
[ad] *NIKHEF, Postbus 41882, NL-1009 DB Amsterdam, The Netherlands*
[ae] *National Technical University, Physics Department, Zografou Campus, GR-15773 Athens, Greece*
[af] *Physics Department, University of Oslo, Blindern, NO-1000 Oslo 3, Norway*
[ag] *Dpto. Fisica, Univ. Oviedo, Avda. Calvo Sotelo s/n, ES-33007 Oviedo, Spain*
[ah] *Department of Physics, University of Oxford, Keble Road, Oxford OX1 3RH, UK*
[ai] *Dipartimento di Fisica, Università di Padova and INFN, Via Marzolo 8, IT-35131 Padua, Italy*
[aj] *Rutherford Appleton Laboratory, Chilton, Didcot OX11 OQX, UK*
[ak] *Dipartimento di Fisica, Università di Roma II and INFN, Tor Vergata, IT-00173 Rome, Italy*
[al] *Dipartimento di Fisica, Università di Roma III and INFN, Via della Vasca Navale 84, IT-00146 Rome, Italy*
[am] *DAPNIA/Service de Physique des Particules, CEA-Saclay, FR-91191 Gif-sur-Yvette Cedex, France*
[an] *Instituto de Fisica de Cantabria (CSIC-UC), Avda. los Castros s/n, ES-39006 Santander, Spain*
[ao] *Dipartimento di Fisica, Università degli Studi di Roma La Sapienza, Piazzale Aldo Moro 2, IT-00185 Rome, Italy*
[ap] *Inst. for High Energy Physics, Serpukov P.O. Box 35, Protvino (Moscow Region), Russian Federation*
[aq] *J. Stefan Institute, Jamova 39, SI-1000 Ljubljana,*
and Laboratory for Astroparticle Physics, Nova Gorica Polytechnic, Kostanjeviska 16a, SI-5000 Nova Gorica,
and Department of Physics, University of Ljubljana, SI-1000 Ljubljana, Slovenia
[ar] *Fysikum, Stockholm University, Box 6730, SE-113 85 Stockholm, Sweden*
[as] *Dipartimento di Fisica Sperimentale, Università di Torino and INFN, Via P. Giuria 1, IT-10125 Turin, Italy*
[at] *Dipartimento di Fisica, Università di Trieste and INFN, Via A. Valerio 2, IT-34127 Trieste,*
and Istituto di Fisica, Università di Udine, IT-33100 Udine, Italy
[au] *Univ. Federal do Rio de Janeiro, C.P. 68528 Cidade Univ., Ilha do Fundão BR-21945-970 Rio de Janeiro, Brazil*
[av] *Department of Radiation Sciences, University of Uppsala, P.O. Box 535, SE-751 21 Uppsala, Sweden*
[aw] *IFIC, Valencia-CSIC, and D.F.A.M.N., U. de Valencia, Avda. Dr. Moliner 50, ES-46100 Burjassot (Valencia), Spain*
[ax] *Institut für Hochenergiephysik, Österr. Akad. d. Wissensch., Nikolsdorfergasse 18, AT-1050 Vienna, Austria*
[ay] *Inst. Nuclear Studies and University of Warsaw, Ul. Hoza 69, PL-00681 Warsaw, Poland*
[az] *Fachbereich Physik, University of Wuppertal, Postfach 100 127, DE-42097 Wuppertal, Germany*

Abstract

Measurements of the trilinear gauge boson couplings $WW\gamma$ and WWZ are presented using the data taken by DELPHI in 1998 at a centre-of-mass energy of 189 GeV and combined with DELPHI data at 183 GeV. Values are determined for Δg_1^Z and $\Delta\kappa_\gamma$, the differences of the WWZ charge coupling and of the $WW\gamma$ dipole coupling from their Standard Model values, and for λ_γ, the $WW\gamma$ quadrupole coupling. A measurement of the magnetic dipole and electric quadrupole moment of the W is extracted from the results for $\Delta\kappa_\gamma$ and λ_γ. The study uses data from the final states $jj\ell\nu$, $jjjj$, ℓX, jjX and γX, where j represents a quark jet, ℓ an identified lepton and X missing four-momentum. The observations are consistent with the predictions of the Standard Model. © 2001 Published by Elsevier Science B.V.

E-mail address: clara.matteuzzi@cern.ch (C. Matteuzzi).
[1] Now at DESY-Zeuthen, Platanenallee 6, D-15735 Zeuthen, Germany.

1. Introduction

The properties of the final state in the reactions $e^+e^- \rightarrow W^+W^-$, $We\nu$ and $\nu\nu\gamma$ are sensitive to trilinear gauge boson couplings [1,2]. This study uses data from the final states $jj\ell\nu$, $jjjj$, ℓX, jjX and γX (where j represents a quark jet, ℓ an identified lepton and X missing four-momentum) taken by the DELPHI detector at LEP in 1998 at a centre-of-mass energy of 189 GeV. The data are used to determine values of three coupling parameters at the WWV vertex (with $V \equiv \gamma, Z$): Δg_1^Z, the difference between the value of the overall WWZ coupling strength and its Standard Model prediction; $\Delta\kappa_\gamma$, the difference between the value of the dipole coupling, κ_γ, and its Standard Model value; and λ_γ, the $WW\gamma$ quadrupole coupling parameter [3].

In the evaluation of the couplings, a model has been assumed [4] in which contributions to the effective WWV Lagrangian from operators describing possible new physics beyond the Standard Model are restricted to those which are CP-conserving, are of lowest dimension ($\leqslant 6$), satisfy $SU(2) \times U(1)$ invariance, and have not been excluded by previous measurements. This leads to possible contributions from three operators, $\mathcal{L}_{W\phi}$, $\mathcal{L}_{B\phi}$ and $\mathcal{L}_W$, and hence to relations between the permitted values of the $WW\gamma$ and WWZ couplings: $\Delta\kappa_Z = \Delta g_1^Z - \frac{s_w^2}{c_w^2}\Delta\kappa_\gamma$ and $\lambda_Z = \lambda_\gamma$, where s_w and c_w are the sine and cosine of the electroweak mixing angle. The parameters we determine are related to possible contributions $\alpha_{W\phi}$, $\alpha_{B\phi}$ and α_W from the three operators given above by: $\Delta g_1^Z = \alpha_{W\phi}/c_w^2$, $\Delta\kappa_\gamma = \alpha_{W\phi} + \alpha_{B\phi}$, and $\lambda_\gamma = \alpha_W$.

The WWV coupling arises in WW production through the diagrams involving s-channel exchange of Z or γ, shown in Fig. 1(a). We study this reaction in the final states $jj\ell\nu$, where one W decays into quarks and the other into leptons, and $jjjj$, where both Ws decay into quarks.

In single W production, the dominant amplitude involving a trilinear gauge coupling arises from the radiation of a virtual photon from the incident electron or positron, interacting with a virtual W radiated from the other incident particle (Fig. 1(b)). This process, involving a $WW\gamma$ coupling, contributes significantly in the kinematic region where a final state electron or positron is emitted at small angle to the beam and is

thus likely to remain undetected in the beam pipe. The decay modes of the W give rise to two final states: that with two jets and missing energy (jjX), and that containing only a single visible lepton coming from the interaction point and no other track in the detector (ℓX).

The trilinear $WW\gamma$ vertex also occurs in the reaction $e^+e^- \rightarrow \nu\nu\gamma$ in the diagram in which the incoming electron and positron each radiate a virtual W at an $e\nu W$ vertex and these two fuse to produce an outgoing photon (Fig. 1(c)). In this process, which leads to a final state, γX, consisting of a single detected photon, the $WW\gamma$ coupling is studied completely independently of the WWZ coupling, as no WWZ vertex is involved.

The next section of this Letter describes the selection of events from the data and the simulation of the various channels involved in the analysis. Section 3 describes the methods used in the determination of coupling parameters. In Section 4 the results from different channels are presented and combined with previously published DELPHI results [2] to give overall values for the coupling parameters. A summary is given in Section 5.

2. Event simulation and selection

In 1998 DELPHI recorded a total integrated luminosity of 155 pb^{-1} at an average centre-of-mass energy of 188.63 ± 0.04 GeV. We characterise here the main features of the selection of events in the final state topologies $jj\ell\nu$, $jjjj$, ℓX, jjX and γX, defined in the previous section. A detailed description of the DELPHI detector may be found in [5], which includes descriptions of the main components of the detector used in this study, namely, the trigger system, the luminosity monitor, the tracking system in the barrel and forward regions, the muon detectors, the electromagnetic calorimeters and the hermeticity counters. The definition of the criteria imposed for track selection and lepton identification and a description of the luminosity measurement are given in [6].

2.1. Event simulation

Various Monte Carlo models were used in the calculation of cross-sections as a function of coupling
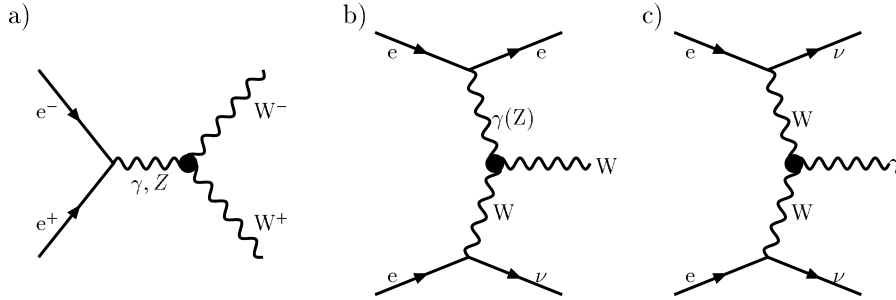
Fig. 1. Diagrams with trilinear gauge boson couplings contributing to the processes studied in this Letter: (a) $e^+e^- \to W^+W^-$, (b) $e^+e^- \to We\nu$, (c) $e^+e^- \to \nu\nu\gamma$.

parameters in the different final states analysed. In the study of the $jj\ell\nu$ and $jjjj$ channels, the four-fermion generators EXCALIBUR [7] and ERATO [8] were used; the studies of the ℓX and jjX final states used calculations based on the program DELTGC [9], cross-checked with GRC4F [10]; DELTGC and NUNUGPV [11] were used to calculate the signals expected in the γX topology. The EXCALIBUR and GRC4F models were interfaced to the JETSET hadronization model [12] tuned to Z data [13]. The study of backgrounds due to $q\bar{q}(\gamma)$ production was made using events from the PYTHIA model [14], while EXCALIBUR was used to study the $q\bar{q}\nu\bar{\nu}$ contribution to the jjX topology, and KORALZ [15], BHWIDE [16] and TEEG [17] were used in the calculation of backgrounds in the ℓX final state. PYTHIA and EXCALIBUR were used in the simulation of events from ZZ production. Two-photon backgrounds were studied using the generators of Berends, Daverveldt and Kleiss [18] and the TWOGAM generator [19]. All of these generators were interfaced to the full DELPHI simulation program [5] except DELTGC and ERATO, which were used only to calculate event weights as a function of the trilinear gauge coupling parameter values (see Section 3).

2.2. Selection of events in the $jj\ell\nu$ topology

Events in the $jj\ell\nu$ topology are characterised by two hadronic jets, a lepton and missing momentum resulting from the neutrino. The lepton may be an electron or muon (coming either from W decay or from the cascade decay of the W through a τ lepton) or, in the case of τ decays, the τ might give rise to

a low multiplicity jet. The major backgrounds come from $q\bar{q}(\gamma)$ production and from four-fermion final states containing two quarks and two leptons of the same flavour.

Events with several hadrons were selected by requiring 5 or more charged particles and a total energy of charged particles recorded in the detector exceeding 15% of the centre-of-mass energy. In the selection of $jj\mu\nu$ and $jje\nu$ events, the candidate lepton was assumed to be the most energetic charged particle in the event; for $jj\tau\nu$ events, the lepton candidates were constructed by looking for an isolated e or μ or a low multiplicity jet.

The selection procedure was identical to that used in our analysis of data at 183 GeV [2], except that, in the selection of electron candidates, the component of the missing momentum transverse to the beam axis was required to be greater than 15 GeV/c and the angle between the electron candidate and the missing momentum was required to exceed 60°.

The efficiency for the selection of $jj\ell\nu$ events was evaluated using fully simulated events to be (79.3 ± 0.2)%, (59.4 ± 0.3)% and (31.7 ± 0.3)% for muon, electron and tau events, respectively. Using data taken only when all essential components of the detector were operational, corresponding to an integrated luminosity of 149 pb^{-1}, 263 muon, 212 electron and 146 tau candidate events were selected. A background contamination of (0.226 ± 0.016) pb was estimated, of which 58% came from the $q\bar{q}(\gamma)$ final state, 22% from Ze^+e^-, 13% from ZZ and $Z\gamma^*$ production and small contributions from non-semileptonic WW events and other sources. The errors on the efficiencies and back-

ground contributions (where given) are statistical errors, resulting from the quantity of simulated data available. The systematic uncertainty resulting from these statistical errors is included in the results shown in Section 4.

2.3. Selection of events in the $jjjj$ topology

The selection of events in the fully hadronic topology followed closely that used in our analysis of data at 183 GeV [2], with only small changes in the values of kinematic cuts.

All detected particles were first clustered into jets using LUCLUS [12] with $d_{join} = 5.5$ GeV/c. Events were accepted if they had at least four jets, with at least four particles per jet. Background from $Z(\gamma)$ events was suppressed by imposing the condition $\sqrt{s'} > 130$ GeV, where $\sqrt{s'}$ is an estimate of the effective collision energy in the (background) $q\bar{q}(\gamma)$ final state after initial state radiation [20]. Events were then forced into a 4-jet configuration and a 4-constraint fit was performed, requiring conservation of four-momentum. Then, in order to suppress the dominant background, which arises from the $q\bar{q}(\gamma)$ final state, the condition $D > 0.0055$ GeV^{-1} was imposed, with $D = \frac{E_{min}}{E_{max}}\theta_{min}/(E_{max} - E_{min})$; E_{min} and E_{max} are the energies of the reconstructed jets with minimum and maximum energy and θ_{min} is the minimum interjet angle in radians. A further fit was then performed on surviving events, imposing four-momentum conservation and requiring the masses of the two reconstructed Ws to be equal. The fit was applied to all three possible pairings of the four jets into two Ws. Fits with reconstructed W mass outside the range $74 < m_W^{rec} < 88$ GeV/c^2 were rejected and, of the remaining fits, the one with minimum χ^2 was accepted.

The efficiency of the selection procedure was evaluated from fully simulated events to be $(75.7 \pm 0.2)\%$. A total of 1130 events was selected from data corresponding to an integrated luminosity of 154.4 pb^{-1}. Background contributions of (1.26 ± 0.02) pb and (0.187 ± 0.007) pb were estimated from $q\bar{q}(\gamma)$ and $jj\ell\nu$ production, respectively. The method used in the analysis of the data to assign the reconstructed jets to W pairs was applied to a sample of simulated events generated with PYTHIA, with only the three doubly resonant CC03 [21] diagrams for WW production present in the production amplitude; in this

model the efficiency of the procedure was estimated to be about 74%.

An additional problem in the analysis of the $jjjj$ state is to distinguish the pair of jets constituting the W^+ decay products from that from the W^-. This ambiguity can be partly resolved by computing jet charges from the momentum-weighted charge of each particle belonging to the jet, $Q_{jet} = \sum_i q_i |p|_i^{0.5} / \sum_i |p|_i^{0.5}$ (where q_i and p_i are the charge and the momentum of the particle and the exponent is chosen empirically), and defining the $W^{\pm}$ charges, Q_{W^+} and Q_{W^-}, as the sums of the charges of the two daughter jets. Following the method of [22], the distribution of the difference $\Delta Q = Q_{W^-} - Q_{W^+}$ was then used to construct an estimator $P_{W^-}(\Delta Q)$ of the probability that the pair with the more negative value of Q_W is a W^-.

An estimate of the efficiency of this procedure was made (for the same sample of simulated WW events as was used to estimate the jet pairing efficiency) by flagging the jet pairs with $\Delta Q < 0$ as W^- and comparing with the generated information. In order to separate this estimate from that for the efficiency of W pair assignment, only events with correct jet pairing were included in the comparison, leading to a value of 77% for the W charge tagging efficiency.

2.4. Selection of events in the ℓX topology

In the selection of candidates for the ℓX final state, events were required to have only one charged particle, clearly identified as a muon from the signals recorded in the barrel or forward muon chambers or as an electron from the signals in the barrel or forward electromagnetic calorimeters. The corresponding selection criteria are described in detail in [6]. In addition, the normal track selections were tightened: the track was required to pass within 1 mm of the interaction point in the xy plane (perpendicular to the beam) and within 4 cm in z. Lepton candidates were also required to have momentum below 75 GeV/c, with a component transverse to the beam above 20 GeV/c. Events were rejected if there was an energy deposition of more than 5 GeV in the barrel or forward electromagnetic calorimeters which was not associated with the charged particle track, or if there was any signal in the hermeticity detectors. In the selection of electron candidates, the ratio of the energy measured in

the electromagnetic calorimeter to the magnitude of the measured momentum was required to exceed 0.7.

Imposing these criteria, 10 events were selected in data in the eX channel, and an efficiency of $(31.2 \pm 3.8)\%$ was obtained for $ee\nu\nu$ production. In the μX channel, 11 events were selected with a calculated efficiency of $(51.2 \pm 6.3)\%$ for $e\mu\nu\nu$ production. In both cases, the efficiency was evaluated in the phase space region defined by the following cuts: one (and only one) lepton was emitted at more than $10.3°$, with an energy between 20 GeV and 75 GeV.

For Standard Model values of the couplings, 8.3 ± 1.0 single electron events were expected, comprising 4.5 events from $ee\nu\nu$ production, 0.3 events from $e\mu\nu\nu$, 0.5 events from $e\tau\nu\nu$ with the τ decay products unseen, 0.2 events from the same final state but with an electron or positron from the τ decay observed in the detector, and 2.8 events from the reaction $e^+e^- \rightarrow e^+e^-\gamma(\gamma)$ with one electron (or positron) and the final state photon(s) unobserved. In the single muon channel, 10.1 ± 1.7 events were expected for Standard Model values of the couplings, comprising 4.2 events from $e\mu\nu\nu$ production, 2.4 events from $ee\mu\mu$ production (coming mainly from two-photon interactions), 0.3 events from $e\tau\nu\nu$, 0.6 events from $\mu\mu\nu\nu$, 0.4 events from $\mu\tau\nu\nu$, 2.1 events from $\mu\mu\gamma$, and a negligible contribution from $\tau\tau\gamma$ production.

All the contributing channels except the Bhabha and Compton backgrounds in the eX final state and the $\mu\mu\gamma$ and $\tau\tau\gamma$ backgrounds and two-photon interactions in the μX channel have a dependence on trilinear gauge boson couplings in their production, and this was taken into account in the subsequent analysis.

2.5. Selection of events in the jjX topology

Events were selected as candidates for the jjX topology if they had total measured transverse momentum greater than 20 GeV/c and invariant mass of detected particles between 45 and 90 GeV/c^2. The detected particles were clustered into jets using LUCLUS with $d_{\text{join}} = 6.5$ GeV/c, and events were accepted if they had two or three reconstructed jets. Surviving events were then forced into a 2-jet configuration.

Events from the WW final state with one W decaying leptonically were suppressed by rejecting events with identified final state leptons (e or μ) of

energy exceeding 12 GeV. In order to suppress the contribution from the $q\bar{q}(\gamma)$ final state, events were rejected if the acoplanarity was greater than $160°$, where acoplanarity is defined as the angle between the projections of the jet momenta on to the plane perpendicular to the beam. In addition, events were rejected if the polar angle of either reconstructed jet was below $20°$, if any charged or neutral particle of momentum exceeding 1 GeV/c was reconstructed within a cone of angle $30°$ about the direction of the missing momentum, or if there was a signal in the hermeticity detectors in a cone of angle $50°$ about the direction of the missing momentum.

Applying these criteria to fully simulated events, an efficiency of $(43.7 \pm 1.5)\%$ was calculated; in the data 64 events were selected. As in the ℓX topology, the efficiency is quoted with respect to a reduced phase space: the electron had to be emitted at less than $10.3°$, the angle between the missing momentum vector (calculated as the negative of the vector sum of the q and $\bar{q}$ momenta) and the beampipe had to be larger than $25°$, the visible transverse momentum had to be at least 15 GeV/c and the visible energy had to be less than 160 GeV. Both momentum and energy here are taken from the four-momenta of the final state q and $\bar{q}$. For the $q\bar{q}$ pair, acollinearity and acoplanarity had to be less than $170°$, and the polar angle of both q and $\bar{q}$ had to exceed $20°$.

For Standard Model values of the couplings, a total of 60.3 ± 0.8 events are expected, comprising 17.0 events from the $q\bar{q}e\nu$ final state with the electron or positron lost in the beam pipe, 5.1 events from $q\bar{q}e\nu$ with the electron or positron elsewhere in the detector, 22.0 events from $q\bar{q}\tau\nu$, 8.1 events from $q\bar{q}\mu\nu$, 3.9 events from $q\bar{q}\nu\nu$, 4.0 events from $q\bar{q}(\gamma)$ production, and 0.2 events from $\gamma\gamma$ interactions. All the processes contributing to the selected sample except $q\bar{q}(\gamma)$ production and two-photon interactions include diagrams with trilinear gauge couplings, and this was taken into account in the subsequent analysis.

2.6. Selection of events in the γX topology

The production of the single photon final state, γX, via a $WW\gamma$ vertex proceeds through the fusion diagram shown in Fig. 1(c), while the dominant process giving rise to this final state, $e^+e^- \rightarrow Z\gamma$ with $Z \rightarrow \nu\bar{\nu}$, involves bremsstrahlung diagrams. The sensitiv-

ity of the γX final states to anomalous $WW\gamma$ couplings is therefore greatest when the photon is emitted at high polar angle. Events were selected if they had a single shower in the barrel electromagnetic calorimeter with $45° < \theta_\gamma < 135°$ and $E_\gamma > 6$ GeV, where θ_γ and E_γ are the polar angle and energy, respectively, of the reconstructed photon. It was also required that no electromagnetic showers were present in the forward electromagnetic calorimeters, and a second shower in the barrel calorimeter was accepted only if it was within 20° of the first one. Cosmic ray events were suppressed by requiring any signal in the hadronic calorimeter to be in the same angular region as the signal in the electromagnetic calorimeter and the electromagnetic shower to point towards the beam collision point [23]. Using these criteria, 145 events were selected from data corresponding to an integrated luminosity of 155 pb^{-1}. The Standard Model expectation is 157.7 ± 3.7 events. Values for the triple gauge boson couplings were fitted in the region $E_\gamma > 50$ GeV, which contained 59% of the events. In this region, an overall selection efficiency of $(54 \pm 4)\%$ was estimated [23], with negligible background contamination.

3. Methods used to determine the couplings

The analysis procedures applied are similar to those used in our previously reported analysis of data at 183 GeV [2], though somewhat different applications of the method of Optimal Observables were used in the analyses of the $jj\ell\nu$ and $jjjj$ final states.

3.1. Optimal Observable analysis of $jj\ell\nu$ and $jjjj$ channels

Data in both the $jj\ell\nu$ and $jjjj$ channels were analyzed using methods based on that of Optimal Observables [24]. The methods exploit the fact that the differential cross-section, $d\sigma/d\vec{V}$, where $\vec{V}$ represents the phase space variables, is quadratic in the trilinear gauge coupling parameters:

$$\frac{d\sigma(\vec{V}, \vec{\lambda})}{d\vec{V}} = c_0(\vec{V}) + \sum_i c_1^i(\vec{V}) \cdot \lambda_i$$
$$+ \sum_{i \leqslant j} c_2^{ij}(\vec{V}) \cdot \lambda_i \cdot \lambda_j, \tag{1}$$

where the sums in i, j are over the set $\vec{\lambda} = \{\lambda_1, \ldots, \lambda_n\}$ of parameters under consideration. It has been shown that the "Optimal Variables" $c_1^i(\vec{V})/c_0(\vec{V})$ and $c_2^{ij}(\vec{V})/c_0(\vec{V})$, approximated for real data by using the reconstructed phase space variables $\vec{\Omega}$ as arguments of the c_1^i and c_2^{ij}, have the same estimating efficiency as can be obtained in unbinned likelihood fits of parameters λ_i to the data [25].

In the determination of a single parameter λ, the joint distribution of the quantities $c_1(\vec{\Omega})/c_0(\vec{\Omega})$ and $c_2(\vec{\Omega})/c_0(\vec{\Omega})$ was compared with the expected distribution, computed from events generated with EXCALIBUR and passed through JETSET and the full detector simulation. An extended maximum likelihood fit, combining the information coming from the shape of the Optimal Variables and from the cross-section, has been carried out. At each stage the simulated data, which had been generated at a few values of the couplings, have been reweighted [26] to the required value of λ using the matrix element calculation of the ERATO generator [8]. In the case of events in the $jj\ell\nu$ topology, the binning in these two variables was made using a multidimensional clustering technique, described in detail in [27]. This is an economical binning method in which the n_d real data points are used as seeds to divide the phase space into an equal number of multidimensional bins. Each simulated event is associated with the closest real event, resulting in an equiprobable division of the space of the Optimal Variables in which it is assumed that the best available knowledge of the probability density function is that of the real data points themselves.

The use of such a technique becomes of particular importance when simultaneous fits to two coupling parameters are performed. The number of Optimal Variables then increases to five: c_1^1/c_0, c_1^2/c_0, c_2^{11}/c_0, c_2^{22}/c_0 and c_2^{12}/c_0, and the use of equal sized bins in a space of this number of dimensions is impractical. For events in the $jj\ell\nu$ topology, an extended maximum likelihood fit was performed over the n_d bins for each pair of coupling parameters (λ_1, λ_2) using this method.

A somewhat different technique was used in 2-parameter fits to data in the $jjjj$ topology. In this case, extended maximum likelihood fits were made to the binned joint distribution of only the first order terms c_1^1/c_0 and c_1^2/c_0 in (1), but an iterative procedure was used, at each stage expanding the expression for the

differential distribution of the phase space variables $\vec{V}$ about the values $(\tilde{\lambda}_1, \tilde{\lambda}_2)$ obtained in the previous iteration:

$$
\begin{aligned}
\frac{d\sigma(\vec{V}, \lambda_1, \lambda_2)}{d\vec{V}} &= c_0(\tilde{\lambda}_1, \tilde{\lambda}_2, \vec{V}) + c_1^1(\tilde{\lambda}_1, \tilde{\lambda}_2, \vec{V})(\lambda_1 - \tilde{\lambda}_1) \\
&\quad + c_1^2(\tilde{\lambda}_1, \tilde{\lambda}_2, \vec{V})(\lambda_2 - \tilde{\lambda}_2) + \cdots.
\end{aligned}
\tag{2}
$$

It has been shown in Ref. [25] that when this iterative procedure has converged sufficiently, the first order terms retain the whole sensitivity of the Optimal Variables to the coupling parameters $\vec{\lambda}$, the contribution from the higher order terms becoming negligible. In practice, this was achieved after about three or four iterations. As an example, Fig. 2 shows the distribution of $c_1^{\Delta g_1^Z}(\vec{\Omega})/c_0(\vec{\Omega})$ for data and for the results of the fit described in the next section.

3.2. Cross-check analysis of $jj\ell\nu$ and $jjjj$ channels

In both the $jj\ell\nu$ and $jjjj$ channels, an additional analysis was performed using more directly measured kinematic variables in order to corroborate results obtained from the methods described above.

In the $jj\ell\nu$ topology, a binned maximum likelihood fit was made to the joint distribution in $\cos\theta_W$, the W^- production angle, and $\cos\theta_\ell$, the polar angle of the produced lepton with respect to the incoming $e^\pm$ of the same sign. In this study, somewhat looser criteria were imposed in the selection of the events, giving a total sample of 743 semileptonic events, with estimated efficiencies of $(79.1 \pm 0.3)\%$, $(67.3 \pm 0.4)\%$ and $(40.4 \pm 0.5)\%$ for muon, electron and tau events, respectively, and an estimated background contamination of 0.49 pb. A 4-constraint kinematic fit was then applied to the events, requiring conservation of four-momentum, and the variables $\cos\theta_W$ and $\cos\theta_\ell$ computed from the fitted four-vectors. The expected number of events in each bin was estimated using events generated with PYTHIA corresponding to the reaction $e^+e^- \rightarrow W^+W^-$ and passed through the full detector simulation procedure. Again, a reweighting technique was used to determine the expected number of events for given values of the coupling parameters. The distributions of $\cos\theta_W$ and $\cos\theta_l$ for real and simulated data are shown in Fig. 3.
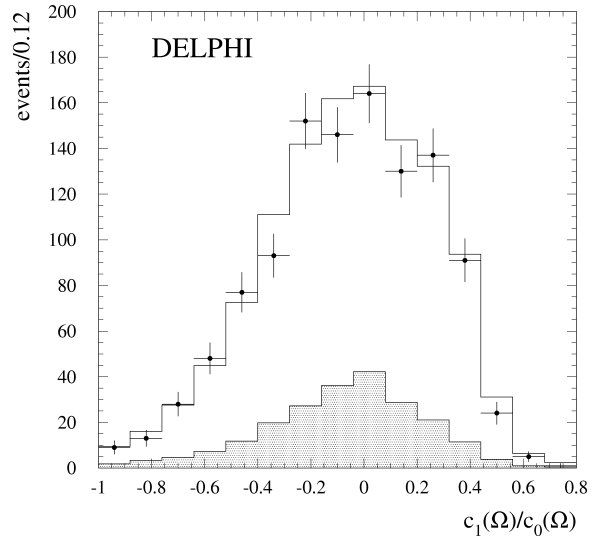

Fig. 2. Distribution of the optimal variable $c_1^{\Delta g_1^Z}(\vec{\Omega})/c_0(\vec{\Omega})$ (defined in the text) for the coupling Δg_1^Z in the $jjjj$ channel from DELPHI data at 189 GeV. The points represent the data and the histogram shows the distribution expected for the fitted value of Δg_1^Z (see Table 1). The shaded area is the estimated background contribution.
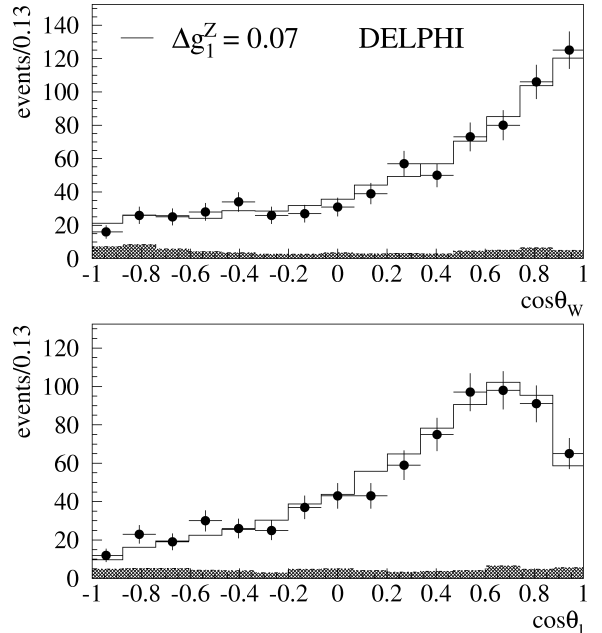

Fig. 3. Distributions in $\cos\theta_W$ and $\cos\theta_\ell$ for $jj\ell\nu$ events ($\ell \equiv e, \mu, \tau$) for DELPHI data, shown as dots, at 189 GeV. The histogram shows the distribution expected for the fitted value of Δg_1^Z (see Table 1). The shaded area is the estimated background contribution.

In the $jjjj$ topology, the second analysis involved a binned extended maximum likelihood fit to the production angular distribution. Events were selected by constructing a probability function from the distributions of eleven kinematic variables, namely: the value of d_{join} in the LUCLUS algorithm when four rather than three natural jets are reconstructed; the sphericity; the angle between the two most energetic jets; the minimal multiplicity in a jet; the second Fox–Wolfram moment; the D variable (defined above); s' (defined above); the fitted W masses; the product of the energy ratios of the two jets in the two reconstructed dijets; the minimal transverse momentum with respect to the beam axis of the 15 most energetic particles in the event; the transverse momentum of the jet pair obtained by forcing the reconstruction of exactly two jets. Using this procedure, a sample of 1331 events was selected with estimated efficiency of $(86.6 \pm 0.2)\%$ and purity of $(74.4 \pm 0.4)\%$. As in the case of the optimal observable analysis of this channel described above, momentum-weighted jet charges were then calculated to try to distinguish the W^+ decay products from those of the W^-. An angular variable $x_g = \cos\theta_W (P_{W^-}(\Delta Q) - P_{W^+}(\Delta Q))$, was constructed from the cosine of the W production angle and the difference in probability of a dijet to come from a W^- or W^+ decay. The experimental distribution of x_g was compared with predictions obtained from events generated with PYTHIA, passed through the full detector simulation procedure, and reweighted in the fit for given values of the coupling parameters.

3.3. Analysis of ℓX, jjX and γX channels

Data in the topologies ℓX and jjX were analysed using maximum likelihood fits to the observed total numbers of events selected, while the γX data were fitted using a binned extended maximum likelihood fit to the distribution of the reconstructed photon energy, E_γ, in the region $E_\gamma > 50$ GeV, which has the maximum sensitivity to anomalous triple gauge boson couplings.

4. Results

The results obtained for the triple gauge boson couplings from the data in each of the final states and using the methods discussed above are shown in Table 1, together with their statistical and systematic errors (see below). The results from all topologies are combined with those previously analysed by DELPHI at 183 GeV and reported in Ref. [2] to give the values of the coupling parameters, their errors and the 95% confidence limits shown in Table 2. In the combination, which is done by adding the individual log-likelihood functions, the results in the $jj\ell\nu$ and $jjjj$ topologies from the methods based on Optimal Observables were used, as these use all the available kinematic information and hence are expected to have greater precision. In the fit to each coupling parameter, the values of the other parameters were held at zero, their Standard Model values. The results of fits in which two of the couplings Δg_1^Z, $\Delta\kappa_\gamma$ and λ_γ were

Table 1
Fitted values of WWV coupling parameters from DELPHI data at 189 GeV using the methods described in the text. The first error given for each value is the statistical error at 68% confidence level (CL), obtained by stepping up 0.5 units from the minimum of the likelihood curve; the second is the systematic error. In the fits to each parameter, the others were set to zero, their Standard Model values

	Δg_1^Z	$\Delta\kappa_\gamma$	λ_γ
$jj\ell\nu$ (Optimal Variables)	$0.00^{+0.08}_{-0.08} \pm 0.02$	$0.28^{+0.35}_{-0.28} \pm 0.10$	$0.06^{+0.09}_{-0.09} \pm 0.02$
$jj\ell\nu$ ($\cos\theta_W, \cos\theta_\ell$)	$0.07^{+0.12}_{-0.11} \pm 0.03$	$0.00^{+0.43}_{-0.24} \pm 0.10$	$0.06^{+0.11}_{-0.10} \pm 0.03$
$jjjj$ (Optimal Variables)	$-0.09^{+0.14}_{-0.12} \pm 0.07$	$0.12^{+0.54}_{-0.31} \pm 0.24$	$0.01^{+0.17}_{-0.15} \pm 0.05$
$jjjj$ ($\cos\theta_W$)	$-0.07^{+0.17}_{-0.13} \pm 0.06$	$0.06^{+0.57}_{-0.31} \pm 0.23$	$-0.05^{+0.19}_{-0.15} \pm 0.06$
ℓX	$-0.45^{+1.35}_{-0.38} \pm 0.21$	$0.23^{+0.27}_{-0.34} \pm 0.19$	$0.48^{+0.33}_{-1.27} \pm 0.21$
jjX	$-0.43^{+1.31}_{-0.39} \pm 0.25$	$0.19^{+0.34}_{-0.57} \pm 0.11$	$0.42^{+0.36}_{-1.20} \pm 0.15$
γX	–	$0.70^{+0.77}_{-0.99} \pm 0.03$	$0.65^{+1.03}_{-1.79} \pm 0.09$

Table 2

Values of WWV coupling parameters combining DELPHI data from various topologies and energies, as described in the text. The second column shows the value of each parameter corresponding to the minimum of the combined negative log-likelihood distribution and its errors at 68% CL. The first error quoted is the combined statistical and uncorrelated systematic error, the second is the total common systematic (see text). The third column shows the 95% confidence intervals on the parameter values, computed by stepping up 2.0 units from the minimum of the likelihood curve. In the fits to each coupling parameter, the other two parameters were set to zero, their Standard Model values

Coupling parameter	Value	95% confidence interval
Δg_1^Z	$-0.02^{+0.07}_{-0.07} \pm 0.01$	$-0.16, 0.13$
$\Delta\kappa_\gamma$	$0.25^{+0.21}_{-0.20} \pm 0.06$	$-0.13, 0.68$
λ_γ	$0.05^{+0.09}_{-0.09} \pm 0.01$	$-0.11, 0.23$

allowed to vary are shown in Fig. 4(a)–(c). In no case is any deviation seen from the Standard Model prediction of zero for the couplings determined.

The results shown in Fig. 4(c) can be transformed to produce estimates for the magnetic dipole moment, μ_W, and the electric quadrupole moment, q_W, of the W boson using the relations

$$\mu_W = \frac{e}{2m_W}\left(g_1^\gamma + \kappa_\gamma + \lambda_\gamma\right) \quad \text{and} \tag{3}$$

$$q_W = -\frac{e}{m_W^2}(\kappa_\gamma - \lambda_\gamma). \tag{4}$$

The resulting two-parameter fit gives the values

$$\mu_W \cdot \frac{2m_W}{e} = 2.22^{+0.20}_{-0.19} \quad \text{and} \tag{5}$$

$$q_W \cdot \frac{m_W^2}{e} = -1.18^{+0.27}_{-0.26}, \tag{6}$$

with the confidence level contours shown in Fig. 4(d). In the derivation of the result for μ_W, the value of g_1^γ, the $WW\gamma$ charge coupling, has been assumed to be unity, as required by electromagnetic gauge invariance. The quantity $(g-2)_W$, derived from the definition of the gyromagnetic ratio of a particle of spin $\vec{s}$, charge Q and mass m, $\vec{\mu} = g\vec{s}\frac{Q}{2m}$, is, therefore, measured to be $(g-2)_W = 0.22^{+0.20}_{-0.19}$.

4.1. Systematic uncertainties

The systematic errors shown in Table 1 and included in the results shown in Table 2 contain con-

tributions from various sources. Table 3 lists the dominant sources of systematic uncertainties for each of the analyses used in the combination. A distinction between systematic errors affecting more than one channel and effects specific to only one channel is made in the combination of the different channels. The list of common systematic effects and the procedure for their combination is given later in this section.

In the $jj\ell\nu$ channel, the dominant effect for Δg_1^Z and λ_γ arises from the uncertainty in the background contamination, where a conservative estimate of $\pm 10\%$ was used. For $\Delta\kappa_\gamma$, the event reconstruction effects give a comparable contribution. Comparisons between Z data and fully simulated events were used to estimate uncertainties of jet and lepton energies and of their angular distributions. These uncertainties were then used to derive an additional smearing for a sample of simulated events, which was then also fitted to the data. The difference arising from fitting this sample and the standard sample is quoted as the event reconstruction uncertainty. A further effect considered was the possibility of misassignment of the lepton charge. This was again studied in Z data, where the fraction of events with misidentified lepton charge was found to be 0.3%. The corresponding systematic effect was calculated by fitting to a simulated sample of $jj\ell\nu$ data with 0.3% of the events randomly assigned the wrong lepton charge. Also included in the table is the systematic error arising from effects of limited Monte Carlo statistics in the evaluation of signal efficiencies.

In the $jjjj$ channel, significant contributions to the systematic error come from the use of simulated event samples with energies different from that of the data, conservatively evaluated by comparing samples generated at 188 and 190 GeV (and labelled "beam energy" in Table 3), and from uncertainties in the jet hadronization model used. The latter were estimated by comparing data sets in which the JETSET and HERWIG [28] fragmentation models were applied to a common set of generated events. The effects of colour reconnection following the SK1 model [29] were investigated by performing a similar comparison between a sample with maximal reconnection probability and the standard unconnected set of JETSET events. As in the analysis of the $jj\ell\nu$ channel, uncertainties due to the background contamination (taken to be $\pm 5\%$) and from limited simulated signal statistics were also taken into account.
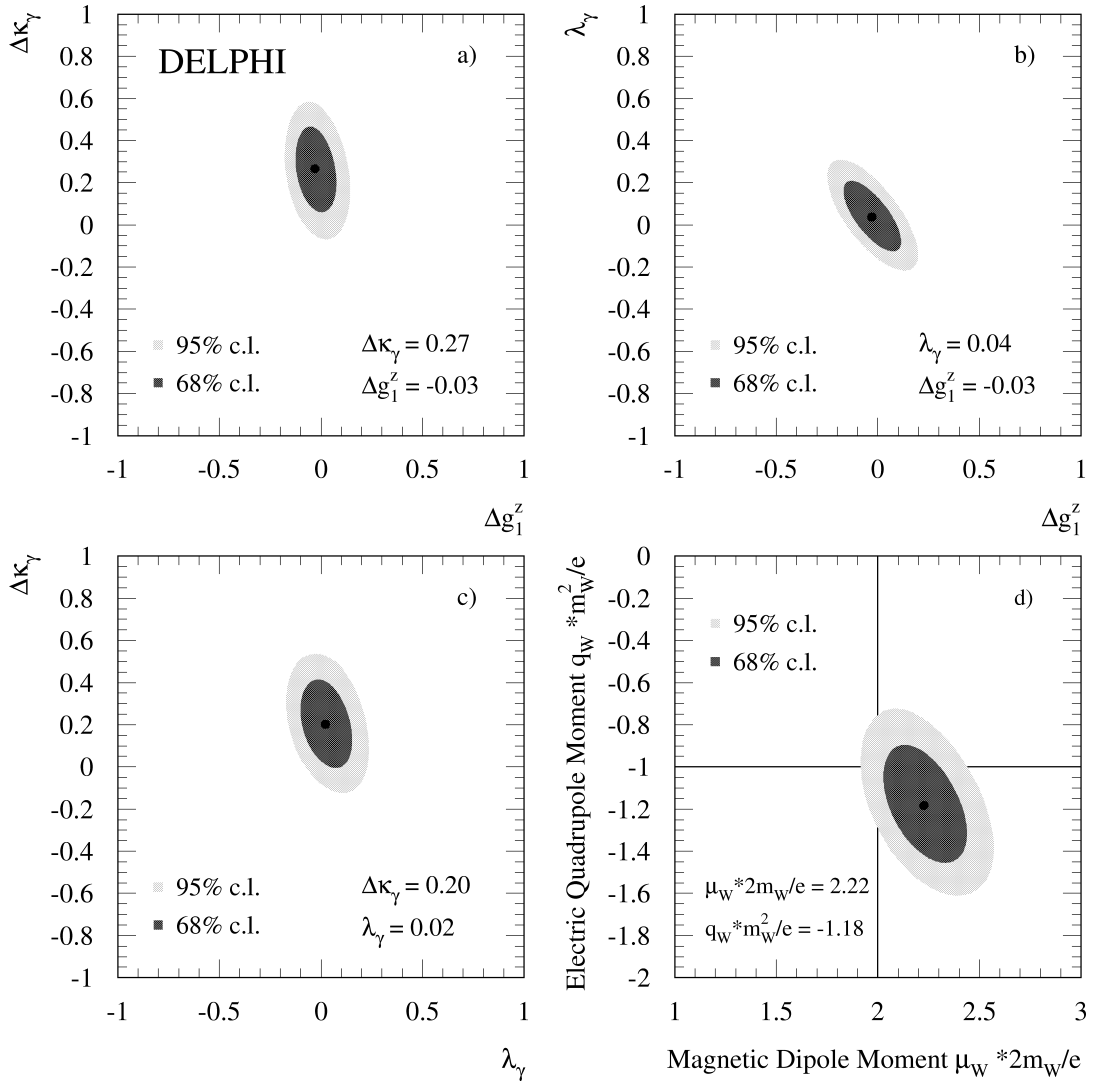
Fig. 4. Results of fits in the planes of the parameters (a) $(\Delta g_1^Z, \Delta \kappa_\gamma)$, (b) $(\Delta g_1^Z, \lambda_\gamma)$, (c) $(\lambda_\gamma, \Delta \kappa_\gamma)$ and (d) (μ_W, q_W) using data from the final states listed in Table 1 combined with DELPHI results at lower energy [2]. In the combination, the analyses of the $jj\ell\nu$ and $jjjj$ final states based on Optimal Observable techniques were used. In each case the third parameter was fixed at its Standard Model value. The values maximizing the likelihood function and the regions accepted at the 68% and 95% confidence levels are shown. The confidence intervals are computed as the contours where the value of the likelihood function is increased by 1.15 units (68% CL) and 3.0 units (95% CL), respectively, from the minimum.

In the single W channels ℓX and jjX, the dominant source of systematic errors is the uncertainty in the efficiency estimation, which is an effect of the limited amount of simulated events available. Limited statistics also affect the background estimation.

In the γX channel, systematic effects play only a minor role. The main systematic contribution origi-

nates from the uncertainty in the energy reconstruction of the barrel electromagnetic calorimeter.

As in our previous analysis [2], the combined results shown in Table 2 include the independent systematic errors from each channel. In addition, systematic effects common to more than one channel, such as the theoretical uncertainty in the WW cross-section, and

Table 3
Main systematic contributions in each analysed channel

Channel	Source and method	Δg_1^Z	$\Delta \kappa_\gamma$	λ_γ
$jj\ell\nu$	Background estimation	±0.013	±0.058	±0.014
	Signal cross-section	±0.002	±0.018	±0.002
	Lepton charge assignment	±0.005	±0.035	±0.009
	Signal MC statistics	±0.005	±0.017	±0.006
	Event reconstruction	±0.005	±0.064	±0.006
	Total $jj\ell\nu$ systematic	±0.017	±0.097	±0.019
$jjjj$	Background estimation	±0.02	±0.05	±0.01
	Signal cross-section	±0.02	±0.13	±0.01
	Colour reconnection	±0.03	±0.07	±0.01
	Fragmentation	±0.01	±0.11	±0.03
	Beam energy	±0.05	±0.11	±0.02
	Total $jjjj$ systematic	±0.07	±0.24	±0.05
ℓX	Background estimation	±0.13	±0.13	±0.12
	Signal cross-section	±0.08	±0.05	±0.07
	Efficiency estimation	±0.15	±0.13	±0.16
	Total ℓX systematic	±0.21	±0.19	±0.21
jjX	Background estimation	±0.03	±0.02	±0.03
	Signal cross-section	±0.08	±0.06	±0.08
	Efficiency estimation	±0.23	±0.09	±0.12
	Total jjX systematic	±0.25	±0.11	±0.15
γX	Energy reconstruction	–	±0.03	±0.09
	Signal cross-section	–	±0.01	±0.01
	Efficiency estimation	–	±0.01	±0.01
	Total γX systematic	–	±0.03	±0.09

the uncertainties in the W mass, in the luminosity measurement and in the LEP beam energy were taken into account separately. The most interesting effect among these correlated systematics is the uncertainty in the WW cross-section calculation, labelled "signal cross-section" in Table 3. To estimate this effect, the cross-section was varied by its theoretical error of ±2%. The effect of this variation is quite small, particularly in the $jj\ell\nu$ channel, which contains the highest sensitivity to the couplings studied. This is reassuring given that

a more precise evaluation of the cross-section is now available [30], which gives a value around 2% lower than currently assumed. As this new cross-section calculation is not yet implemented in our event generators, we have used the old calculations and quote a systematic error which covers the difference between the two cross-section values. Uncertainties in the differential cross-sections that could arise from the difference between our Monte Carlo generators and the new generators, or from the theoretical uncertainty in the new calculations are the subject of an ongoing LEP-wide study and are not taken into account in the results presented here.

The common effects were evaluated individually for each final state and then added with weights derived from the statistical precision of the individual channels with respect to each coupling.

5. Conclusions

Values for the WWV couplings Δg_1^Z, $\Delta \kappa_\gamma$ and λ_γ have been derived from an analysis of DELPHI data at 189 GeV. The results have been combined with previously published values from DELPHI data at 183 GeV, giving an overall improvement in precision by a factor of about two over that of the 183 GeV data [2]. The results of the 2-parameter fit to the couplings $\Delta \kappa_\gamma$ and λ_γ have been used to derive values for the magnetic dipole and electric quadrupole moments of the W and for the W gyromagnetic ratio.

There is no evidence for deviations from Standard Model predictions in any of the results obtained.

References

[1] DELPHI Collaboration, P. Abreu et al., Phys. Lett. B 423 (1998) 194.

[2] DELPHI Collaboration, P. Abreu et al., Phys. Lett. B 459 (1999) 382.

[3] K. Hagiwara, R. Peccei, D. Zeppenfeld, K. Hikasa, Nucl. Phys. B 282 (1987) 253.

[4] G. Gounaris, J.-L. Kneur, D. Zeppenfeld, in: G. Altarelli, T. Sjöstrand, F. Zwirner (Eds.), Physics at LEP2, CERN 96-01, Vol. 1, 1996, p. 525.

[5] DELPHI Collaboration, P. Aarnio et al., Nucl. Instrum. Methods A 303 (1991) 233;
DELPHI Collaboration, P. Abreu et al., Nucl. Instrum. Methods A 378 (1996) 57;
P. Chochula et al., Nucl. Instrum. Methods A 412 (1998) 304.

[6] DELPHI Collaboration, P. Abreu et al., E. Phys. J. C 2 (1998) 581.

[7] F.A. Berends, R. Kleiss, R. Pittau, EXCALIBUR, in: G. Altarelli, T. Sjöstrand, F. Zwirner (Eds.), Physics at LEP2, CERN 96-01, Vol. 2, 1996, p. 23.

[8] C.G. Papadopoulos, Comput. Phys. Commun. 101 (1997) 183.

[9] O.P. Yushchenko, V.V. Kostyukhin, DELTGC: A program for four-fermion calculations, DELPHI note DELPHI 99-4 PHYS 816 (1999).

[10] J. Fujimoto et al., GRC4F, in: G. Altarelli, T. Sjöstrand, F. Zwirner (Eds.), Physics at LEP2, CERN 96-01, Vol. 2, 1996, p. 30.

[11] G. Montagna et al., Nucl. Phys. B 452 (1995) 161.

[12] T. Sjöstrand, PYTHIA 5.7 / JETSET 7.4, CERN-TH.7112/93, 1993.

[13] DELPHI Collaboration, P. Abreu et al., Z. Phys. C 73 (1996) 11.

[14] T. Sjöstrand, PYTHIA 5.719 / JETSET 7.4, in: G. Altarelli, T. Sjöstrand, F. Zwirner (Eds.), Physics at LEP2, CERN 96-01, Vol. 2, 1996, p. 41.

[15] S. Jadach, B.F.L. Ward, Z. Wąs, Comput. Phys. Commun. 79 (1994) 503.

[16] S. Jadach, W. Placzek, B.F.L. Ward, Phys. Lett. B 390 (1997) 298.

[17] D. Karlen, Nucl. Phys. B 289 (1987) 23.

[18] F.A. Berends, P.H. Daverveldt, R. Kleiss, Comput. Phys. Commun. 40 (1980) 271, 285, 309.

[19] S. Nova, A. Olshevski, T. Todorov, in: G. Altarelli, T. Sjöstrand, F. Zwirner (Eds.), Physics at LEP2, CERN 96-01, Vol. 2, 1996, p. 224.

[20] P. Abreu et al., Nucl. Instrum. Methods A 427 (1999) 487.

[21] W. Beenakker, F.A. Berends, in: G. Altarelli, T. Sjöstrand, F. Zwirner (Eds.), Physics at LEP2, CERN 96-01, Vol. 1, 1996, p. 79.

[22] ALEPH Collaboration, R. Barate et al., Phys. Lett. B 422 (1998) 369.

[23] DELPHI Collaboration, P. Abreu et al., E. Phys. J. C 17 (2000) 53.

[24] M. Diehl, O. Nachtmann, Z. Phys. C 62 (1994) 397.

[25] G.K. Fanourakis, D. Fassouliotis, S.E. Tzamarias, Nucl. Instrum. Methods A 414 (1998) 399;
G.K. Fanourakis, D. Fassouliotis, A. Leisos, N. Mastroyiannopoulos, S.E. Tzamarias, Nucl. Instrum. Methods A 430 (1999) 474.

[26] G.K. Fanourakis, D. Fassouliotis, S.E. Tzamarias, Nucl. Instrum. Methods A 412 (1998) 465.

[27] G.K. Fanourakis, D. Fassouliotis, A. Leisos, N. Mastroyiannopoulos, S.E. Tzamarias, Nucl. Instrum. Methods A 430 (1999) 455.

[28] G. Abbiendi, I.G. Knowles, G. Marchesini, M.H. Seymour, L. Stanco, B.R. Webber, Comput. Phys. Commun. 67 (1992) 465.

[29] T. Sjöstrand, V.A. Khoze, Z. Phys. C 62 (1994) 281;
T. Sjöstrand, V.A. Khoze, Phys. Rev. Lett. 72 (1994) 28.

[30] A. Denner et al., Phys. Lett. B 475 (2000) 127;
S. Jadach et al., Precision predictions for (un)stable W^+W^- pair production at and beyond LEP2 energies, hep-ph/0007012, 2000;
M. Grünewald, G. Passarino et al., Four-fermion production in electron–positron collisions, hep-ph/0005309, 2000.